Received: 8 July 2022 | Revised: 14 November 2022 | Accepted: 21 December 2022

DOI: 10.1002/jrs.6490

RESEARCH ARTICLE

Journal of RAMAN SPECTROSCOPY WILEY

Identification of histidine-Ni (II) metal complex by Raman spectroscopy

Petra Pál[1] | **Miklós Veres**[2] | **Roman Holomb**[2,3] | **Melinda Szalóki**[4] | **István Csarnovics**[1] | **Attila Gábor Szöllősi**[5]

[1]Department of Experimental Physics, University of Debrecen, Debrecen, Hungary

[2]Institute for Solid State Physics and Optics, Wigner Research Centre for Physics, Budapest, Hungary

[3]Department of Information and Operating Systems and Technologies, Uzhhorod National University, Uzhhorod, Ukraine

[4]Department of Biomaterials and Prosthetic Dentistry, Faculty of Dentistry, University of Debrecen, Debrecen, Hungary

[5]Institute of Immunology, Faculty of General Medicine, University of Debrecen, Debrecen, Hungary

Correspondence
Petra Pál, Department of Experimental Physics, University of Debrecen, Debrecen, Hungary.
Email: pal.petra@science.unideb.hu

Funding information
National Research, Development and Innovation Fund of Hungary, Grant/Award Numbers: TKP2021-EGA-20, TKP2020-NKA-04; New National Excellence Program of the Ministry of Human Capacities, Grant/Award Numbers: ÚNKP-21-5-DE-464, ÚNKP-22-3-II-DE-53, ÚNKP-22-5-DE-407; National Research, Development, and Innovation Fund of Hungary; János Bolyai Research Scholarship of the Hungarian Academy of Sciences, Grant/Award Number: BO/348/20

Abstract

Metal ions such as nickel have a strong binding affinity to amino acids and form metal complexes of different geometry. This complex formation is influenced by many factors among others the kind of reactants and their relative concentrations, pH, and its effect on the net charge of the amino acid molecule. In this work, the formation of the histidine-nickel (II) complex in different conditions was examined by Raman spectroscopy. In addition to the experiments, density functional theory (DFT) calculations on histidine-nickel complexes were performed in order to elucidate the complex formation mechanism and optimal geometry of the structures as well as to investigate their vibrational properties. The Raman measurements showed double peaks at 1272 and 1297 cm^{-1}, and triple peaks at 1322, 1336, and 1355 cm^{-1} that belong to the metal complex. The geometry optimizations and total energy calculations of His-Ni (II) complex revealed that the octahedral geometry and the triplet spin state of Ni ion is the energetically favorable structure. This metal complex is formed through the nitrogen atom of the imidazole side chain, the nitrogen atom of the terminal amino group, and the oxygen atom of the carboxyl group. Experiments with pH revealed that the alkaline pH favors while the change of the concentration of the metal ions does not affect the the His-Ni (II) complex formation.

KEYWORDS

His-Ni (II) complex, histidine, metal complex, nickel (II), Raman spectroscopy

1 | INTRODUCTION

The role of metals is becoming increasingly important in today's society, but the growing amounts of metals and metal-containing compounds present in our everyday lives can also lead to potential environmental problems. The leaching of metal-containing compounds and substances into the soil and groundwater is remarkable; thereby, higher and higher volumes of metal ions are found in plants, animals, and drinking water. This can potentially affect humans, as the entry of metal ions into the bloodstream is thought to lead to neurological diseases, cell damage, and oncogenesis.[1] On the other hand, metal ions play an important role in many biological processes, which is why the study of metal complexes in bioligands has received increasing attention in recent decades. The study of the interaction of peptides and amino acids with essential and toxic elements is a particularly popular topic in bioorganic chemistry, as proteins are the major binding sites for metal ions in biological systems.[2]

Metal ions may play a role in the development of neurodegenerative diseases. These disorders affect the nerve cells in the human brain, leading to mental and physical degradation of the patient. The most well known of them are, for example, Alzheimer's and Parkinson's disease.[1,3,4] In each case, a protein[5–8] is closely related to the pathology of these diseases, and there is increasing evidence of the importance of the role of metals.[9,10] While essential metal ions are key to the normal functioning of the brain, neurodegenerative disorders are mediated or triggered by their imbalance, which can result in the misfolding and agglomeration of proteins, leading to changes in critical biological systems, and triggering a series of events that ultimately lead to neurodegeneration and cell death.[11]

Nickel in its various alloys and compounds is widely distributed in nature. It is essential for most living organisms, but in larger quantities, it is considered as toxic and carcinogenic agent to the human body. In this regard, inhalation of nickel-containing aerosols and the load caused by drinking water are generally less important. Rather, nickel ingested orally with nutriment is the most important route of exposure. The absorption of nickel depends on its physicochemical form, and its water-soluble compounds (chloride, nitrate, sulphate) are more easily absorbed. In general, due to its slow absorption from the stomach and intestine, ingested nickel compounds are rarely toxic due to their low dose. However, when administered orally in high doses (>0.5 g), some forms of nickel may be acutely toxic to the human body. Nickel also causes skin irritation, and skin allergy, pulmonary fibrosis, respiratory cancer, and iatrogenic nickel poisoning may also occur in human organisms exposed to highly nickel-contaminated environments.[12–15]

The toxic functions of nickel are likely to result primarily from its ability to replace other metal ions in enzymes and proteins or to bind to cellular compounds containing O, S, and N atoms, which will then be inhibited. Metal ions, including Ni (II) ions, are thought to play a role in the development of neurodegenerative diseases.[1,12,14]

Peptides, which are essential components of the living cell mass, are multifaceted and potent ligands that form a stable complex with the vast majority of metal ions. Divalent transition metal ions (e.g., copper (II), nickel (II), zinc (II), cobalt (II), and cadmium (II)) are the most common examples of the formation of these complexes.[16]

Peptides are made up of α-amino acids.[17] In terms of their structural features α-amino acids always contain a terminal amino group (-NH_2) and a terminal carboxyl group (-COOH), as well as a sidechain incorporating different functional groups. These amino and carboxyl groups are capable of binding the metal ion, and the side chain may be involved in this process if it contains a donor group capable of attachment to the metal ion.[2,17] For example, alanine contains no or weakly coordinating side-chain donor groups, whereas cysteine (thiol) and histidine (imidazole-N) contain highly coordinating ones.[2,16,18] Ni (II) ions can form stable complexes with most peptides and proteins as well. They bind to the nitrogen atom of the terminal amino, amide, or imidazole groups. In terms of the structure of the formed metal complexes, the octahedron and plane square geometry is the most common.[13]

The importance of histidine interactions with transition metal ions, including Ni (II), has long been recognized in biological systems.[19] Interactions between Ni (II) ions and histidine bound in different coordination have been widely reported.[13,20–23] In the acidic pH range, the imidazole nitrogen of histidine is the primary binding site. As the pH is increased (shifted to the basic range), the donor atoms in histidine are deprotonated, so the molecule may contain three possible coordination sites. If increasing the pH further, the oxygen atom of the carboxyl group and the nitrogen of the amino group are released, which may also participate in the complex formation, in addition to the nitrogen of the imidazole. The Ni (II) ions present in the system can result in the formation of two types of metal complexes (His-Ni and His-Ni-His),[19,24,25] as it was confirmed by a combination of potentiometric titrations and spectroscopic (ultraviolet–visible [UV-vis] and circular dichroism) methods.[2,13,21–23,26–28]

In addition, new methods have also appeared in the last few decades that can be used to detect possible

His-Ni binding sites. An example is an interferometric technique that works on the optical principle, which enables the detection of bonds between ions and proteins, and the number and strength of binding sites can be determined, and rate constants can also be calculated.[29,30] Furthermore, Ni-NTA (nitrilotriacetic acid) surfaces are suitable for the specific binding of proteins that are connected to the Ni-NTA surface via the N- or C-terminal through their histidine-labeled part. With this, various protein–protein and protein-DNA interactions can be studied.[30,31]

Metal ions play an important role in biological systems, especially among proteins; it is essential to further study the relationship between these metal ions and proteins and to detect and identify the formed metal complex efficiently, quickly, and easily.

Raman spectroscopy is a widely used technique allowing the identification of molecules and their structure, chemical bonds and bond order, intermolecular interactions, and so forth. Being a branch of vibrational spectroscopy, this method is also useful to identify different compounds and biological materials based on their unique vibrations. Nowadays this method is widely used in materials science, medicine, archeology, and even criminal investigations. It should be also noted that the Raman measurements are nondestructive and do not require special sample preparation. Therefore, Raman spectroscopy is suitable for measurements of heat-sensitive biological samples, such as proteins, too.[32,33]

This study is aimed to investigate the formation of the His-Ni (II) complex in different conditions using Raman spectroscopy. The use of this technique has not been reported before. The complex formation was experimentally studied under different conditions, including the excess of the metal and the histidine in the solution, as well as the modification of the pH. In addition, molecular modeling and DFT calculations were performed to verify the complex formation and to facilitate the interpretation of the Raman results.

2 | MATERIALS AND METHODS

2.1 | Sample preparation

L-histidine (His; Sigma-Aldrich, Japan) and nickel (II) chloride hexahydrate ($NiCl_2{\cdot}6H_2O$; Sigma-Aldrich, France) were used as received without further purification. The aqueous solutions of crystalline L-histidine and nickel (II) chloride hexahydrate were prepared in ultrapure water. The concentration of histidine was 0.05 mol/dm^3 in all cases and of the $NiCl_2$ solutions were the following: 5 mol/dm^3, 0.5 mol/dm^3, 0.05 mol/dm^3, 0.005 mol/dm^3; 37% w/w HCl (VWR, Hungary) and 1% w/w NaOH solution, prepared from solid NaOH (VWR, Hungary), were used for pH adjustment. For investigation of histidine nickel (II) complex formation in acidic circumstances, 37% w/w was added to the solution, followed by the addition of $NiCl_2$ solution, in a 1:1:1 volume ratio, respectively. The investigation of complex formation in basic circumstances was performed by adding 1% w/w NaOH solution and then $NiCl_2$ solution to His solution in a 1:1:1 volume ratio. The pH of solutions was measured by an Orion 2-Star pH meter (Thermo Scientific, Singapore, Ayer Rajah Crescent).

2.2 | Raman measurements

Raman measurements were performed using a Horiba LabRam (France) and a Renishaw inVia (UK) Raman spectrometer. Silicone wells (Sigma Aldrich) attached to a silicon wafer were used to contain the samples. The volume of a well was 5 μl, which was filled with the sample and covered with a calcium fluoride (CaF_2) cover plate to prevent solvent evaporation and to ensure the stability of the volume and the concentration of the tested liquids during the measurements.

During the Raman measurements, the excitation light was focused under the cover plate with a 50× objective. All spectra were excited using a diode laser operating at 532 nm. The incident laser power was limited to 5 mW. The acquisition time was 30 s with five accumulations (i.e., the total exposure time was 150 s).

2.3 | Theoretical calculations

Based on the earlier studies,[13,16,18] the structure of the resulting metal-histidine complex may have an octahedral geometry, involving also two or three water molecules, respectively.[1] Possible binding sites in the histidine molecule include the nitrogen atom of the imidazole ring, the oxygen atom of the carboxyl group, and the nitrogen atom of the amino group. Taking these into account, the following single and dual His-Ni complex geometries were modeled for the theoretical calculations, which are shown in Figure 1.

The self-consistent density functional theory (DFT) field method using the hybrid B3LYP functional consisting of a linear combination of the pure corrected exchange functional by Becke[34] and the three-parameter gradient-corrected correlation functional by Lee et al.[35] were used for all calculations using the Gaussian-09 program package.[36] The triple zeta valence (TZV) Pople 6-311++G(d,p) basis set was utilized for all atoms.[37] No

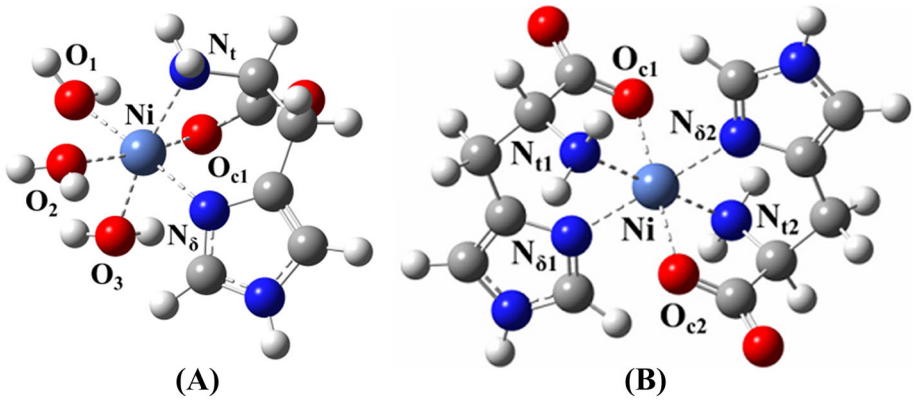

FIGURE 1 Optimized geometry of gas-phase single (A) and dual (B) histidine-nickel complexes together with labels and numbering of the selected atoms [Colour figure can be viewed at wileyonlinelibrary.com]

TABLE 1 Interatomic distances and total energies (E^{tot}) of single and dual His-Ni complexes optimized using gas-phase and SMD models

Singel His-Ni (II)			Dual His-Ni (II)		
	Distances (Å)			Distances (Å)	
Atom labels	Gas phase	SMD	Atom labels	Gas phase	SMD
Ni-O_{c1}	1.98	2.08	Ni-$O_{c1/2}$	2.04	2.11
Ni-N_{δ}	2.07	2.08	Ni-$N_{\delta1/2}$	2.18	2.17
Ni-N_t	2.09	2.09	Ni-$N_{t1/t2}$	2.13	2.12
E^{tot} (a.u.)	−2285.9253	−2286.0551	E^{tot} (a.u.)	−2605.08311	−2605.16951

geometrical constraints were applied to the model during minimization of the total energy of histidine-Ni complexes performed using the Berny optimization algorithm.

Initial geometry optimizations were performed on the gas-phase of histidine-Ni complex models. The explicit solvent model consisting of three water molecules was used for single histidine-Ni complex (Figure 1A). In addition, the solvation model assuming the water medium as an infinite continuum having dielectric and hydrophobic properties like that of the water molecule was used. The solvation of both single- and dual histidine-Ni complexes was implicitly described using the universal continuum solvation model based on density (SMD) developed by Truhlar et al.[38] The total energies and optimal interatomic distances of single and dual histidine-nickel complexes calculated using a gas phase and continuum solvation models are tabulated in Table 1.

Subsequent frequency calculations performed using the same method and basis set verified the optimized complex as a true minimum energy structure. All calculated vibrational mode frequencies were scaled by using an empirical factor of 0.97. The calculated Raman modes of the models were used to simulate the Raman spectra of the histidine-nickel complexes using a Lorentz-shape function with intensity being proportional to the calculated Raman activity and with full width at half-maximum (FWHM) of 8 cm^{-1}, modeling the natural bandwidth of the experimental spectra.

3 | RESULTS AND DISCUSSION

3.1 | Raman measurements and theoretical calculations

As a starting point, an aqueous solution of histidine and $NiCl_2$ at a concentration of 0.05 mol/dm^3 was used for the experiments. The first step was to measure the histidine (His) solution, whose Raman spectrum is shown in Figure 2 (red line). All peaks of histidine are narrow, typical for amino acid molecules (it should be noted that the broad band in the 1500–1800 cm^{-1} region is related to water).

The structure of histidine is shown in Figure 2. The sum formula of the molecule is $C_6H_9N_3O_2$, and it contains carbon, nitrogen, oxygen, and hydrogen atoms. Table 2 summarizes the observed peaks in the Raman spectrum, together with the reference peak positions published earlier,[39] and their associated vibrations. The Raman spectrum is dominated by different C-C, C-N, C-H, and N-H vibrations.

Then Ni (II) ions in 0.05 mol/dm^3 concentration were added to the 0.05 mol/dm^3 concentration of the histidine sample in a 1:1 volume ratio. Figure 2 compares the spectra of Ni (II), His, and His-Ni (II) solutions. Figure 2 shows the difference between the His + Ni (II) and the His spectra due to the addition of Ni (II) ions. The main differences were observed in the range of 1000–1500 cm^{-1}. Figure 3 shows this range of the two spectra. Several significant discrepancies can be observed in this region.

It can be observed that the peaks at 1159, 1234, 1267, 1287, and 1495 cm^{-1} have disappeared, whereas the intensities of the bands at 1196, 1323, 1354, 1414, 1443, and 1575 cm^{-1} decreased. These changes indicate the alteration of the structure of the histidine molecule and suggest the formation of the nickel-histidine complex. This is also confirmed by the appearance of new peaks in the spectrum of His-Ni (II) at 1272, 1297, and 1336 cm^{-1}. Thus, we hypothesize that the double peaks at 1272 and 1298 cm^{-1}, as well as those triple peaks at 1322, 1337,

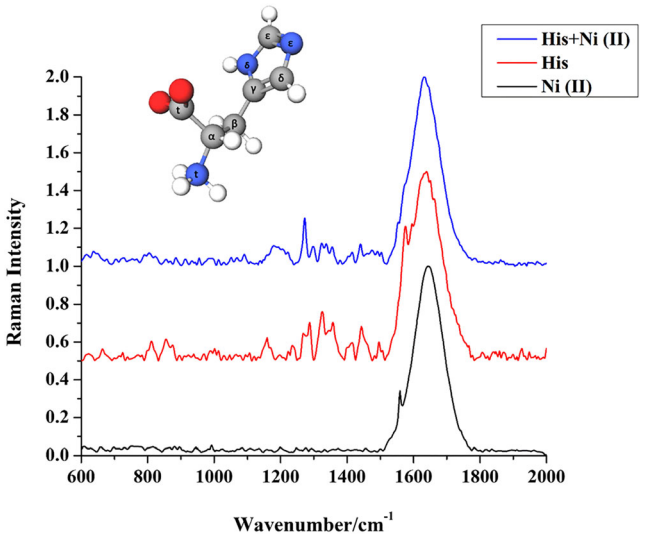

FIGURE 2 Measured Raman spectra of nickel, histidine, and His-Ni (II) solutions, and the structure of histidine [Colour figure can be viewed at wileyonlinelibrary.com]

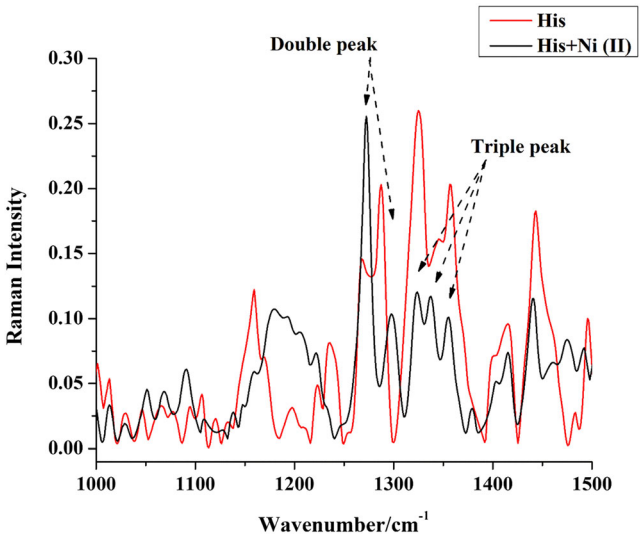

FIGURE 3 Measured Raman spectra of His and His-Ni (II) solutions in the Raman shift range of 1000–1500 cm^{-1} [Colour figure can be viewed at wileyonlinelibrary.com]

TABLE 2 Raman peak positions and assignments for histidine. The atom markings are the same as in Figure 2

Measured Raman peak (cm^{-1})	Reference Raman peak (cm^{-1})[39]	Assignment
855	855	ω (C_ε-H)
873	874	ω (C_δ-H), τ (C_γ-C_δ)
990	993	C_α-C_β
1014	1010	C_γ-N_δ-C_ε, N_δ-C_ε-N_ε
1159	1160	N_ε-C_ε, C_γ-N_ε, N_ε-C_ε-H
1196	1193	$N_tH_3^+$asym. rock., C_β-C_α-H_α
1235	1236	$N_tH_3^+$asym. rock., C_β-twist
1267	1268	N_δ-C_ε-H, C_γ-C_δ-H
1287	1287	C_γ-N_δ, C_γ-N_ε, C_β-rock., C_β-C_γ
1325	1324	$N_tH_3^+$asym. rock., C_β-rock., C_t-C_α-H
1357	1357	N_δ-C_ε, C-twist., C_γ-N_δ
1414	1412	N_t-C_α-H_α, C_β-C_α-H, C_β-rock
1443	1441	C_tOO^- sym. st., C_α-C_t
1495	1516	N_ε-C_ε, N_δ-C_ε-H, N_ε-C_ε-H
1575	1576	C_γ-C_δ, C_β-C_γ, N_δ-C_γ-C_δ

and 1355 cm^{-1} can be related to the His-Ni (II) complex. In addition, it can also be concluded that the N_δ atom of the imidazole ring (disappearance of the peaks at 1267 and 1287 cm^{-1}), the N_t atom of the amino-containing side chain (disappearance of the peaks at 1134 and 1323 cm^{-1}, respectively), and the O atom of the carboxyl group (decrease in the intensity of the peak at 1443 cm^{-1}) are involved in the bond formation with Ni (II) ions, thereby forming the His-Ni (II) complex. To verify our hypothesis, theoretical calculations were performed to obtain the Raman lines of the His-Ni (II) complex.

The models of His-Ni interactions consist of a single and a dual histidine-Ni complex (Figure 1) adopting the octahedral-type geometry. Recently, it was found that the higher spin state is energetically preferable for Ni^{2+} cation in such complex.[2] Therefore, all the calculations described here were performed using the triplet state. In this geometric arrangement, the metal ion is bound by histidine through the N_δ-Ni-O_c/N_t atoms (Figure 1A). As mentioned earlier (Figure 3), the double and triple peaks observed in the 1000–1500 cm^{-1} spectral range may be important. Therefore, Figure 4 shows a detailed comparison of simulated Raman spectrum of single His-Ni (II) ion complex in octahedral triplet form calculated by using the SMD model and experimentally measured Raman spectrum of histidine-nickel solution.

A good agreement is observed between experimental and theoretical spectra. As can be seen from Figure 4, the double (indicated with red) and triple (indicated with green) peaks are characteristics for both spectra.

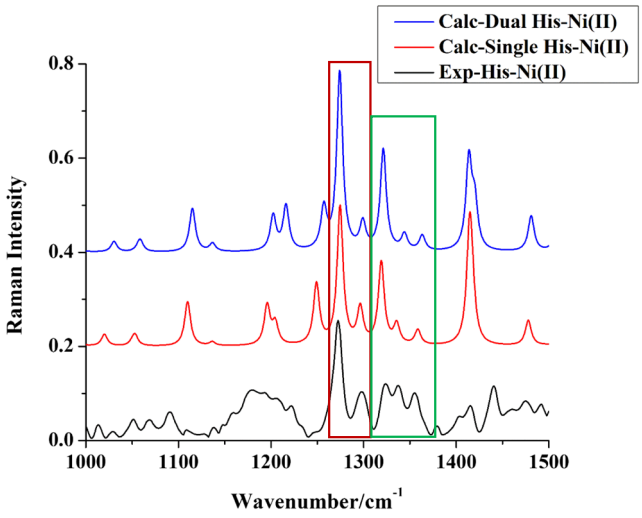

FIGURE 4 Comparison of experimental Raman spectra of His-Ni solution and calculated spectra of single and dual His-Ni (II) complexes in the Raman spectral range of 1000–1500 cm^{-1} [Colour figure can be viewed at wileyonlinelibrary.com]

According to the experimental measurements, the positions of double peaks are 1272 and 1297 cm^{-1}, whereas the triple peaks are situated at 1323, 1337, and 1355 cm^{-1}. The theoretical predictions for these peaks are 1274 and 1296 cm^{-1} and 1319, 1335, and 1358 cm^{-1}, respectively. In addition to these bands, the two spectra show several matches, such as the peaks at 1051, 1109, 1194, 1204, 1414, and 1474 cm^{-1}.

The formation of a dual histidine-nickel complex is also possible. Therefore, such possibility was also considered during the modeling and the additional DFT calculations were performed on dual His-Ni (II) complex (His-Ni-His). The optimal geometry structure of this complex is shown in Figure 1B. The model consists of an octahedral (triplet state) conformation in geometrical arrangements allowing metal ion to interact with histidine molecules through the N_δ-Ni-O_c/N_t atoms.

Simulated Raman spectrum of His-Ni-His complex was compared with experimental and theorical (single His-Ni (II)) spectra of the complex also shown in Figure 4. As can be seen in Figure 4, the theoretical spectrum (blue spectra) of this conformation shows a high degree of similarity with experimental one. The double (indicated with red) and triple peaks (indicated with green) connected with the interaction of metal ion with amino acid are appear in the simulated Raman spectrum of this complex geometry. Also, there are other similarities between the experimental spectrum and that predicted for such octahedral arrangement.

From these findings, it can be concluded that the formation of a metal-histidine complex through the N_δ, O_c, and N_t atoms is more likely. The resulting complex forms an octahedral conformation in which the Ni ions are in the triplet spin state. Furthermore, if we examine the theoretically calculated Raman spectra of the single His-Ni (II) complex and the double His-Ni (II) complex, it can be seen that the spectra of the two geometric arrangements show a high degree of similarity. In terms of the intensity of the double peaks, they are almost identical in both the experimental and theoretical spectra. In the case of the triple peak, there are differences in intensity, and a smaller frequency shift can be observed in the positions of some bands, but we cannot distinguish between these two forms based on such small differences. Thus, we can assume that both forms are present in the system.

3.2 | Effect of pH on the formation of the His-Ni (II) complex

There is considerable research on the study of the His-Ni (II) complex. Most of the works examine the formation

and properties of the complex under neutral or alkaline pH conditions.[16,18,21,40] The molecular structure and the charge of histidine molecules are changing by the pH shift that influences functional groups involved in the binding of Ni ions and thus in the formation and stability of the complex. Therefore, the next step was to change the pH value and to investigate the features of the His-Ni (II) complex.

Histidine is unique among the amino acids because at physiological pH it can exist in neutral or positively charged forms.[41] Acid dissociation constants (pK) of histidine molecule correspond to three coordination groups, namely carboxyl (pK_1), amino (pK_2), and imidazole (pK_R) group. At a pH superior to pK ($pK_R = 6$), at pH 7, the amine group (N_ε-$C_\delta H$) of the imidazole side chain is uncharged making amino acid less hydrophilic. In this case, the terminal amino group in the molecule is in protonated (-$N_tH_3^+$) and the carboxyl group is in deprotonated (-COO^-) forms (third His molecule structure in Figure 5). At a pH superior to pK_2 ($pK_2 = 9.17$) the net charge of His molecule is −1 (fourth His molecule structure in Figure 5). At a pH inferior to pK_R, the N_ε atom of the imidazole side chain picks up an H^+ ion (proton) and therefore becomes positively charged and highly hydrophilic. At a pH inferior to pK_1 ($pK_1 = 1.82$) the carboxylic group also accepts a proton (first His molecule structure in Figure 5).

Since Raman spectroscopy is very sensitive to protonation/deprotonation forms of the molecules, it can be expected that the change in the pH will be reflected in the Raman spectra as well.

3.2.1 | Acidic pH

The pH of His solution was shifted to the acidic range by the addition of 37% w/w HCl, followed by $NiCl_2$ solution in a 1:1:1 volume ratio. The pH of the acidic mixture was 1, which is below pK_1 and the net charge of His molecule is +2.

Figure 6A. compares the Raman spectra of His, His + Ni (II), His + HCl, and His + HCl + Ni (II), respectively. The spectrum of histidine changed due to the addition of the acid. The 1159 cm^{-1} peak disappeared, and a new band appeared at 1189 cm^{-1} and the 1235 cm^{-1} peak associated with NtH_3^+ vibration also vanished. Instead of the bands at 1268 and 1287 cm^{-1}, a peak appeared at 1271 cm^{-1}. In addition, new bands can be seen at 1330 and 1369 cm^{-1}. Furthermore, the 1414 cm^{-1} peak disappeared, the intensity of the 1444 cm^{-1} peak decreased, and the intensity of the 1495 cm^{-1} peak increased.

Based on these findings, it can be concluded that the disappearance of the peaks at 1159, 1268, and 1287 cm^{-1} and the increase of the intensity of the 1271 and 1495 cm^{-1} peaks all confirm the protonation of the N_ε atom of the imidazole ring in acidic medium (see Figure 6A). Furthermore, the changes in the bonds of the

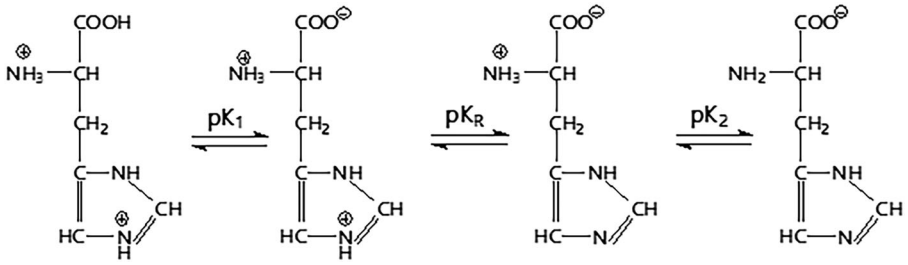

FIGURE 5 Changes in the structure of the histidine molecule at different pH values

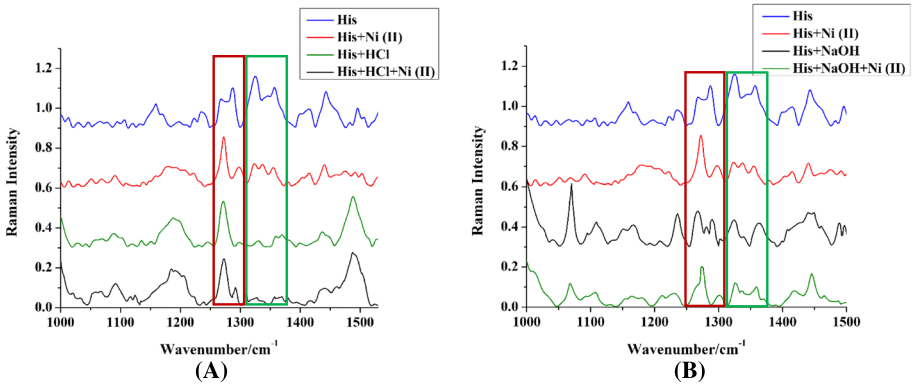

FIGURE 6 (A) Raman spectra of histidine and histidine-Ni (II) in acidic and neutral medium. (B) Raman spectra of histidine and histidine-Ni (II) in alkaline and neutral medium [Colour figure can be viewed at wileyonlinelibrary.com]

N_t atom in the amino group are supported by the appearance of the 1189 cm^{-1} peak and the disappearance of the 1235 and 1414 cm^{-1} peaks. Also, protonation of the carboxyl group may cause a decrease in the intensity of the peaks at 1330 and 1369 cm^{-1} and the decrease of the band at 1444 cm^{-1}, respectively.

Ni (II) solution was added to His solution after its acidification. No remarkable changes were observed in the spectrum, and the triple and double peaks, described earlier, do not appear, from which it can be concluded that the acidic medium does not favor the formation of the His-Ni (II) complex.

3.2.2 | Alkaline pH

A similar procedure has been performed with an alkaline pH medium. First, 1 w/w% NaOH and then $NiCl_2$ solution were added to the solution in a 1:1:1 volume ratio. The measured pH of this mixture was 12.63, which is above pK_2 ($pK_2 = 9.17$) and the net charge of the histidine molecule is −1. In this case, only the carboxyl group is present in the molecule in deprotonated form, as shown in Figure 5. The Raman spectra of His, His + Ni (II), His + NaOH, and His + NaOH + Ni (II) solutions are shown in Figure 6B. It is clear from Figure 6B that the spectrum of histidine also changed under the influence of alkali, so there was also a change in its structure. The intensities of the 1069 and 1107 cm^{-1} peaks increased. Instead of the 1158 cm^{-1} band, a double peak appeared at 1150 and 1160 cm^{-1}. In addition, the intensities of the features at 1236 and 1267 cm^{-1} also increased, whereas those at 1287 and 1325 cm^{-1} decreased, and at 1489 cm^{-1} a band appeared.

Based on these observations, it can be concluded that the N_t atom of the amino group in the histidine molecule is neutral at pH 12.63, so the bonds of this N atom change due to deprotonation, which appears as the increased intensity of the 1069, 1170, 1236 cm^{-1} peaks, and the decrease of the 1325 cm^{-1} band. The 1150 and 1160 cm^{-1} peaks appear instead of the 1158 cm^{-1} band, the increase in the intensity of the 1267 cm^{-1} peak, the decrease in the intensity of the 1287 cm^{-1} band, and the appearance of the 1489 cm^{-1} peak all confirm the changes of N_ε atom of the imidazole ring. In an alkaline medium, the imidazole ring is neutral (Figure 5). After the addition of Ni (II) solution to the alkaline His solution, the Raman spectrum of alkaline His changed to a greater extent compared with the spectra of acidic His. In addition to the double peak attached to the complex, the triple peak also appears, from which it can be concluded that the alkaline medium is favorable for complex formation.

3.3 | Effect of concentration of Ni (II) ions on the formation of the His-Ni (II) complex

In the following experiments, the concentration of $NiCl_2$ was changed, whereas the concentration of the histidine solution remained constant (0.05 mol/dm^3). As previously presented, the formation of a single His-Ni (II) or double His-Ni (II) complex cannot be determined from the Raman data due to the great similarity of their spectra. In the following experiments, the concentration of $NiCl_2$ was varied to analyze how the concentration of Ni (II) ions affects the complex formation. The concentrations of the $NiCl_2$ solutions were as follows: 5 mol/dm^3, 0.5 mol/dm^3, 0.05 mol/dm^3, and 0.005 mol/dm^3. The His:Ni (II) volume ratios were 1:1 in each case. Figure 7 shows the effect of Ni (II) ion concentration on the His-Ni (II) complex formation.

It can be seen in Figure 7 that when the ratio of the concentration is 1:1 (blue curve) and 1:10 (red curve), the intensity of the peaks is nearly the same. This indicates that the complexes are formed in the same amount at both volume ratios. If the concentration of Ni (II)-ions is low (0.005 mol/dm3), compared with His solution (that means the histidine is in excess), the complex is formed in the same way—the triple peaks appear, but also the characteristic peaks of histidine are present (green line). If the concentration of Ni (II)-ions is higher (5 mol/dm^3, black line), the complex is also formed but the intensities of the peaks of the His-Ni (II) complex decrease thanks to the excess of Ni (II) ions.

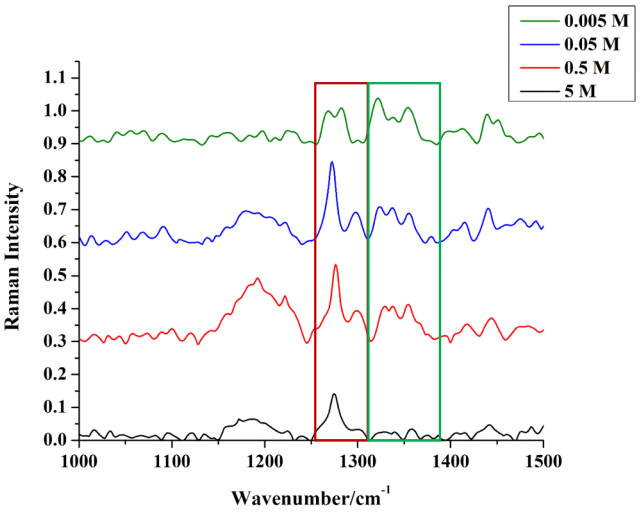

FIGURE 7 Effect of Ni (II) ion concentration on the Raman spectrum of His-Ni (II) complex formation [Colour figure can be viewed at wileyonlinelibrary.com]

4 | CONCLUSION

The His-Ni (II) complex formation in different conditions was investigated in detail using Raman spectroscopy. The experiments were completed by DFT calculations on two types (single and dual) of octahedral coordinated histidine-Ni complexes. A good accordance was observed between the simulated Raman spectra of His-Ni complexes and the experimental Raman spectrum of the histidine-nickel complex solution. The results show that the nitrogen atom of the imidazole, the nitrogen atom of the terminal amino group, and the oxygen atom of the carboxyl group are involved in metal ion binding (Nδ-Ni-Oc/Nt). The detailed analysis of unique Raman bands (double peaks at 1272 and 1297 cm^{-1} and triple peaks at 1322, 1336, and 1355 cm^{-1}) characteristic of His-Ni complexes implies that Raman spectroscopy can successfully be used to identify molecular complexation in this system as well as to study the interactions between the Ni ion and histidine molecules.

It was found that alkaline pH (pH was changed from 1 to 12) favors the formation of the His-Ni (II) complex. Above pK_2, the number of possible coordination sites increases as the donor atoms in the amino acid are deprotonated, which promotes the binding of the metal ion.

The effect of metal ion concentration on the histidine-nickel complex formation was also studied. For nearly equal concentration ratio between Ni cation and histidine, the His-Ni complex formation is fully completed, leaving no excess of either. In addition to the metal-histidine complex, the excess of amino acid can be detected by Raman spectroscopy when the concentration of metal ions is decreased. However, the high concentration (5 M) of metal ions in histidine-nickel solution leads to the suppression of the Raman signal related to the complex.

In summary, it can be concluded that the metal complexes formed with histidine Ni (II) ions can be examined and detected by Raman spectroscopy. This can be important in research areas where fast and simple testing of metal complexes is essential. This research can be useful, for example, for the detection of nickel sensitivity, where the complexes formed by Ni (II) with proteins are important, or the importance of the role of metal ions in the field of neurodegenerative disease research. In addition, it is worth mentioning the possibility of testing different his-tagged DNA chains. In addition, the investigation of metal complexes with Raman spectroscopy can also be used in other areas. An example of such an area is catalytic hydrogen storage, where metal complexes are used as catalysts.

ACKNOWLEDGEMENTS

Petra Pál is grateful for the support from the ÚNKP-22-3-II-DE-53 New National Excellence Program of the Ministry for Culture and Innovation from the source of the National Research, Development and Innovation Fund. Project TKP2020-NKA-04 has been implemented with support provided by the National Research, Development, and Innovation Fund of Hungary, financed under the 2020-4.1.1-TKP2020 funding scheme. Istvan Csarnovics is grateful for the support of the János Bolyai Research Scholarship of the Hungarian Academy of Sciences (BO/348/20) and the support through the New National Excellence Program of the Ministry of Human Capacities (ÚNKP-22-5-DE-407). Project no. TKP2021-EGA-20 (Biotechnology) has been implemented with the support provided from the National Research, Development and Innovation Fund of Hungary, financed under the TKP2021-EGA funding scheme.

ORCID

Petra Pál https://orcid.org/0000-0003-1423-090X

REFERENCES

[1] L. M. Franklin, S. M. Walker, G. Hill, *J. Mol. Model.* **2020**, *26*, 116.
[2] E. Farkas, I. Sóvágó, in *Amino Acids, Peptides and Proteins*, *Vol. 41* (Eds: M. Ryadnov, F. Hudecz), Royal Society of Chemistry, Great Britain, Cambridge **2017**, 100.
[3] Y. Christen, *Am. J. Clin. Nutr.* **2000**, *71*, 621S.
[4] R. R. Crichton, D. T. Dexter, R. J. Ward, *Coord. Chem. Rev.* **2008**, *252*, 1189.
[5] J. Collinge, *Annu. Rev. Neurosci.* **2001**, *24*, 519.
[6] M. G. Spillantini, M. L. Schmidt, V. M.-Y. Lee, J. Q. Trojanowski, R. Jakes, M. Goedert, *Nature* **1997**, *388*, 839.
[7] M. G. Spillantini, R. A. Crowther, R. Jakes, M. Hasegawa, M. Goedert, *Proc. Natl. Acad. Sci.* **1998**, *95*, 6469.
[8] S. Sinha, I. Lieberburg, *Proc. Natl. Acad. Sci.* **1999**, *96*, 11049.
[9] D. R. Brown, *Metallomics* **2010**, *2*, 186.
[10] B. N. Dugger, D. W. Dickson, *Cold Spring Harb. Perspect. Biol.* **2017**, *9*, 1.
[11] K. A. Jellinger, *Int. Rev. Neurobiol.* **2013**, *110*, 1.
[12] M. Cempel, G. Nikel, *Polish J. Environ. Stud.* **2006**, *15*, 375.
[13] C. Conato, H. Kozłowski, J. Swiatek-Kozłowska, P. Młynarz, M. Remelli, S. Silvestri, *J. Inorg. Biochem.* **2004**, *98*, 153.
[14] T. P. Coogan, D. M. Latta, E. T. Snow, M. Costa, A. Lawrence, *CRC Crit. Rev. Toxicol.* **1989**, *19*, 341.
[15] P. Grandjean, *IARC Sci. Publ.* **1984**, *53*, 469.
[16] I. Sóvágó, C. S. Kállay, K. Várnagy, *Coord. Chem. Rev.* **2012**, *256*, 2225.
[17] G. Wu, *Amino Acids* **2009**, *35*, 1.
[18] H. Kozłowski, W. Bal, M. Dyba, T. Kowalik-Jankowska, *Coord. Chem. Rev.* **1999**, *184*, 319.
[19] L. E. Valenti, C. P. De Pauli, C. E. Giacomelli, *J. Inorg. Biochem.* **2006**, *100*, 192.
[20] H. Sigel, R. B. Martin, *Chem. Rev.* **1982**, *82*, 385.

[21] G. FBryce, F. R. N. Gurd, *J. Biol. Chem.* **1966**, *241*, 1439.
[22] W. Bal, H. Kozlowski, R. Robbins, L. D. Pettit, *Inorg. Chim. Acta* **1995**, *231*, 7.
[23] M. A. Zoroddu, T. Kowalik-Jankowska, H. Kozlowski, H. Molinari, K. Salnikow, L. Broday, M. Costa, *Biochim. Biophys. Acta* **2000**, *1475*, 163.
[24] R. J. Sundberg, R. B. Martin, *Chem. Rev.* **1974**, *74*, 471.
[25] N. Lihi, M. Lukács, D. Szűcs, K. Várnagy, I. Sóvágó, *Polyhedron* **2017**, *133*, 364.
[26] P. J. Morris, R. Bruce Martin, *J. Inorg. Nucl. Chem.* **1970**, *32*, 2891.
[27] R. W. Hay, M. M. Hassan, C. You-Quan, *J. Inorg. Biochem.* **1993**, *52*, 17.
[28] K. Vassilev, M. Dimitrova, S. Turmanova, R. Milina, *Synth. React. Inorg. Metal-Org. Nano-Metal Chem.* **2013**, *43*, 243.
[29] H. Jankovics, B. Kovacs, A. Saftics, T. Gerecsei, É. Tóth, I. Szekacs, F. Vonderviszt, R. Horvath, *Sci. Rep.* **2020**, *10*, 22253.
[30] H. N. Daghestani, B. W. Day, *Sensors* **2010**, *10*, 9630.
[31] G. J. Wegner, H. J. Lee, G. Marriott, R. M. Corn, *Anal. Chem.* **2003**, *75*, 4740.
[32] R. R. Jones, D. C. Hooper, L. Zhang, D. Wolverson, V. K. Valev, *Nanoscale Res. Lett.* **2019**, *14*, 231.
[33] E. S. Allakhverdiev, V. V. Khabatova, B. D. Kossalbayev, E. V. Zadneprovskaya, O. V. Rodnenkov, T. V. Martynyuk, G. V. Maksimov, S. Alwasel, T. Tomo, S. I. Allakhverdiev, *Cell* **2022**, *11*, 386.
[34] A. D. Becke, *Phys. Rev. A* **1998**, *38*, 3098.
[35] C. Lee, W. Yang, R. G. Parr, *Phys. Rev. B* **1988**, *37*, 785.
[36] M. J. Frisch, G. W. Trucks, H. B. Schlegel, G. E. Scuseria, M. A. Robb, J. R. Cheeseman, G. Scalmani, V. Barone, B. Mennucci, G. A. Petersson, H. Nakatsuji, M. Caricato, X. Li, H. P. Hratchian, A. F. Izmaylov, J. Bloino, G. Zheng, J. L. Sonnenberg, M. Hada, M. Ehara, K. Toyota, R. Fukuda, J. Hasegawa, M. Ishida, T. Nakajima, Y. Honda, O. Kitao, H. Nakai, T. Vreven, J. A. Montgomery Jr., J. E. Peralta, F. Ogliaro, M. Bearpark, J. J. Heyd, E. Brothers, K. N. Kudin, V. N. Staroverov, R. Kobayashi, J. Normand, K. Raghavachari, A. Rendell, J. C. Burant, S. S. Iyengar, J. Tomasi, M. Cossi, N. Rega, J. M. Millam, M. Klene, J. E. Knox, J. B. Cross, V. Bakken, C. Adamo, J. Jaramillo, R. Gomperts, R. E. Stratmann, O. Yazyev, A. J. Austin, R. Cammi, C. Pomelli, J. W. Ochterski, R. L. Martin, K. Morokuma, V. G. Zakrzewski, G. A. Voth, P. Salvador, J. J. Dannenberg, S. Dapprich, A. D. Daniels, O. Farkas, J. B. Foresman, J. V. Ortiz, J. Cioslowski, D. J. Fox, *Gaussian 09, Revision A.02*, Gaussian, Inc, Wallingford CT **2009**.
[37] V. A. Rassolov, J. A. Pople, M. A. Ratner, T. L. Windus, *J. Chem. Phys.* **1998**, *109*, 1223.
[38] A. V. Marenich, C. J. Cramer, D. G. Truhlar, *J. Phys. Chem. B* **2009**, *113*, 6378.
[39] F. Pflüger, B. Hernández, M. Ghomi, *J. Phys. Chem. B* **2010**, *114*, 9072.
[40] A. A. Gesawat, M. A. Ahmed, F. Shakeel, *J. Chil. Chem. Soc.* **2010**, *55*, 304.
[41] A. Patronov, E. Salamanova, I. Dimitrov, D. R. Flower, I. Doytchinova, *Curr. Comput.-AidedDrugDes.* **2014**, *10*, 41.

How to cite this article: P. Pál, M. Veres, R. Holomb, M. Szalóki, I. Csarnovics, A. G. Szöllősi, *J Raman Spectrosc* **2022**, 1. https://doi.org/10.1002/jrs.6490